

Alma Mater Studiorum Università di Bologna
Archivio istituzionale della ricerca

Engineering the Fullerene-protein Interface by Computational Design: The Sum is More than its Parts

This is the final peer-reviewed author's accepted manuscript (postprint) of the following publication:

Published Version:

Trozzi, F., Marforio, T.D., Bottoni, A., Zerbetto, F., Calvaresi, M. (2017). Engineering the Fullerene-protein Interface by Computational Design: The Sum is More than its Parts. ISRAEL JOURNAL OF CHEMISTRY, 57(6), 547-552 [10.1002/ijch.201600127].

Availability:

This version is available at: <https://hdl.handle.net/11585/616843> since: 2018-12-18

Published:

DOI: <http://doi.org/10.1002/ijch.201600127>

Terms of use:

Some rights reserved. The terms and conditions for the reuse of this version of the manuscript are specified in the publishing policy. For all terms of use and more information see the publisher's website.

This item was downloaded from IRIS Università di Bologna (<https://cris.unibo.it/>).
When citing, please refer to the published version.

(Article begins on next page)

This is the accepted manuscript version of the following article:

Francesco Trozzi, Tainah Dorina Marforio, Andrea Bottoni, Francesco Zerbetto, Matteo Calvaresi, Engineering the Fullerene-Protein Interface by Computational Design: The Sum is More than its Parts, *Isr. J. Chem.*, **2017**, 57, 547 – 552.

Dipartimento di Chimica “G. Ciamician”, Alma Mater Studiorum, Università di Bologna, via F. Selmi 2, 40126 Bologna, Italy

Which has been published in final form at:

<https://dx.doi.org/10.1002/ijch.201600127>

This article may be used for non-commercial purposes in accordance with Wiley Terms and Conditions for Use of Self-Archived Versions.

© 2017 Wiley-VCH Verlag GmbH & Co. KGaA, Weinheim

Engineering the Fullerene-Protein Interface by Computational Design: The Sum is More than its Parts

Francesco Trozzi,⁺ Tainah Dorina Marforio,⁺ Andrea Bottoni, Francesco Zerbetto,*
Matteo Calvaresi*

Dipartimento di Chimica “G. Ciamician”, Alma Mater Studiorum, Università di
Bologna, via F. Selmi 2, 40126 Bologna, Italy

⁺ These authors contributed equally to this work

E-mail: francesco.zerbetto@unibo.it; matteo.calvaresi3@unibo.it

Abstract

Of all the amino acids, the surface of π -electron conjugated carbon nanoparticles has the largest affinity for tryptophan, followed by tyrosine, phenylalanine, and histidine. In order to increase the binding of a protein to a fullerene, it should suffice to mutate a residue of the site that binds to the fullerene to tryptophan, Trp. Computational chemistry shows that this intuitive approach is fraught with danger. Mutation of a binding residue to Trp may even destabilize the binding because of the complicated balance between van der Waals, polar and non-polar solvation interactions.

Keywords.

Nano-bio interface; fullerene, lysozyme, computational design, binding pocket optimization.

1. Introduction

Understanding the interactions at the nano–bio interface is the first step for the safe use of nanotechnology and for the design of nanomaterial for biological applications.¹ Engineering specific interactions between proteins and nanoparticles will allow development of new applications and design innovative nanomachines, sensors, and theranostic platforms.²

Computational design offers opportunities for engineering protein structure and function.³ Binding pocket optimization allows the design of specific interactions between proteins and ligands.³ In these designs, an existing protein is generally used as a scaffold, and its binding pocket is modified to tune the interaction with the target ligand.³ Generally, the optimization of the protein binding pocket is carried out considering small molecules as ligands.

The ability of carbon nanoparticles and fullerenes to interact with proteins was demonstrated for the first time by pioneering work that reported the C₆₀ inhibiting activity on HIV-proteases.⁴ Protein interactions with fullerene-based compounds were later identified in many other systems both computationally⁵⁻¹⁹ and experimentally.²⁰⁻⁴¹ In the study of protein-nanoparticles interactions, it is often hard to ascertain if the measured interactions are due to (i) the formation of a well-defined 1:1 adduct, (ii) binding of the protein with aggregates, or (iii) average effects deriving by the binding of the nanoparticle(s) to multiple protein binding sites. To achieve binding pocket optimization it is necessary to work with a well-defined system where the interaction between the nanoparticle and the protein binding pocket is highly specific and localized. For this reason, we choose here C₆₀@lysozyme that we recently characterized.²⁴ NMR chemical shift perturbation analysis unambiguously

identified a fullerene-protein binding pocket in solution.²⁴ The NMR and spectroscopic data showed that lysozyme forms a truly stoichiometric 1:1 adduct with C₆₀ where lysozyme maintains its tridimensional structure with only a few well-identified residues that are structurally perturbed.²⁴

Molecular dynamics (MD) simulations already provided information regarding interactions of fullerenes and carbon nanoparticles with proteins showing the dynamics at the molecular level and addressing the effects of surface chemistry on the adsorption of proteins.^{42,43} Using the MM-PB(GB)SA protocol to analyze the MD trajectories, we recently described a computational procedure that provides a detailed analysis of the various components of the binding energy and quantifies the interactions between the protein and the π electron conjugated surface at the level of individual residues.^{6,8} This approach allowed us to identify “hot” and “cold” spots for the interaction. Different interactions such as π - π stacking interactions, hydrophobic interactions, surfactant-like interactions, electrostatic interactions govern the wealth of structures that appear when proteins and fullerenes interact. The per-residue decomposition of $\Delta G_{\text{binding}}$ of C₆₀@lysozyme helped us in understanding the roles of the various aminoacids of the protein.⁶ The calculations emphasized the role of Trp residues (Trp62 and Trp63) in the binding process.⁶ It is well-known that protein adsorption onto carbon nanoparticles improves with the increase of the content of aromatic residues in the protein sequence.⁴⁴ Among the aromatic amino acids, tryptophan possesses the highest affinity for carbon nanoparticles, followed by tyrosine, phenylalanine, and histidine.⁴⁴ The π -stacking contacts between the indolic group of Trp residues and the carbon cage, which are identified in the C₆₀@Lysozyme complex govern the interactions between lysozyme and C₆₀.⁶ This π -stacking interaction may be sandwich-like, as for Trp62, or T-shape-like, as for Trp63.⁶

In this paper, we endeavor to engineer the fullerene-lysozyme interface by computational design, in order to provide guidelines for the optimal binding of proteins to fullerenes.

2. Results and Discussion

Lysozyme mutants. In C_{60} @lysozyme, the per-residue decomposition analysis of the $\Delta G_{\text{binding}}$ ⁶ already showed that there are seven more residues that have an interaction energy with C_{60} that is higher than 1 kcal mol⁻¹. In addition to the two Trp residues (Trp 62 and Trp 63), these residues make up the fullerene binding pocket of wild-type lysozyme (See Figure 1).⁶

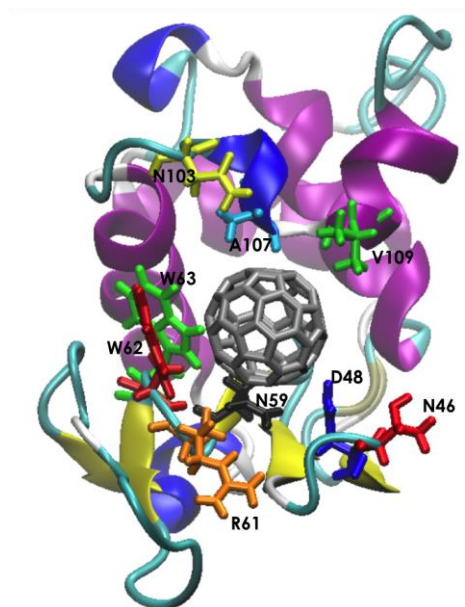


Figure 1. Fullerene binding pocket of wild-type lysozyme. The more interacting residues ($E_{\text{interact}} > 1$ kcal mol⁻¹) of wild-type lysozyme with C_{60} are in licorice.

Since tryptophan is the aminoacid that shows the highest values of interaction with C_{60} , we mutate *in silico*, one at a time, the other 7 “binding” residues of the wild-type lysozyme binding pocket (Figure 1) to Trp residues. This procedure generates 7 lysozyme mutants (see Table 1, Figures S1-S7 for a 3D representation of the mutants). Then we study the effect of the mutation on the structure of the complex

and on the $\Delta G_{\text{binding}}$, with the aim to optimize the interaction energy of the protein with the C_{60} .

Table 1. Lysozyme mutants and interaction energies of the newly introduced tryptophan (kcal/mol).

Wild-Type Lysozyme	Lysozyme Mutant	Interaction energy with C_{60}
WT-N46	N46W	-2.0
WT-D48	D48W	-2.8
WT-N59	N59W	-4.1
WT-R61	R61W	-3.0
WT-N103	N103W	-1.4
WT-A107	A107W	-2.9
WT-V109	V109W	-1.3

MD and MM-GBSA analysis of the C_{60} @Lysozyme-mutants complexes.

Starting from the NMR data²⁴ and from the previous calculation about C_{60} @lysozyme,⁶ we construct all the different complexes between C_{60} and the lysozyme mutants. Subsequently, we carry out a scoring of the interaction energy (see Computational Details) for all the complexes. The estimation of the binding energy between the lysozyme mutants and C_{60} is performed using a molecular mechanics/Generalized-Born Surface Area (MMGBSA) analysis of the MD individual trajectories. We compare the calculated interaction energies with the results obtained for the wild-type lysozyme ($\Delta\Delta G_{\text{binding}}$) in order to estimate the effect of the mutation on the $\Delta G_{\text{binding}}$ (Figure 2).

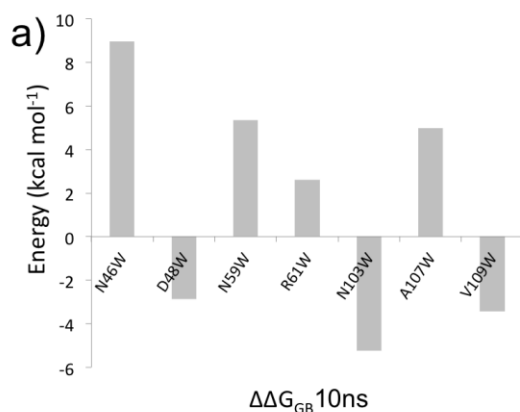


Figure 2. Overall variation of the interaction energy $\Delta\Delta G_{\text{binding}}$ of C_{60} with lysozyme mutants compared to Wild-Type Lysozyme.

In principle, it could be expected that the mutation with Trp would increase $\Delta G_{\text{binding}}$ of C_{60} to the protein. There are, however, four cases where the mutation worsens the interaction of the protein with the fullerene cage, namely N46W, N59W, N61W, N107W. In three cases, D48W, N103W, V109W, $\Delta G_{\text{binding}}$ increases, as expected.

This result confirms that the simple presence of amino acids with a strong tendency to bind carbon nanoparticles does not guarantee strong binding of proteins to a fullerene. The three-dimensional arrangement of the amino acid side chains around C_{60} is crucial. Interestingly, the mutations that show the larger variation of $\Delta G_{\text{binding}}$ involve an arginine (N46 and N103). The two variations have a different sign.

In order to analyze in detail the structural and energetic effects caused by these two cases, we carry out longer MD simulations of 100 ns.

Binding of C_{60} with wild-type lysozyme and the N103W, N46W mutants

The role of surface complementarity in the binding of C_{60} with proteins is known to be crucial.^{6,8} In fact, the most important energetic terms, i.e. van der Waals interactions and energy desolvation are roughly proportional to the variation of the Solvent Accessible Surface Area, ΔSASA , that is a measure of the surface

complementarity.^{6,8} This phenomenon is similar to the well-known encapsulation of C₆₀ by macrocyclic receptors,⁴⁵ where concave-convex complementarity is the driving force to fullerene binding.⁴⁵ To provide an initial estimate of the effect of the mutations on $\Delta G_{\text{binding}}$, we can compare ΔSASA in the mutants and in the wild type lysozyme, upon binding with the C₆₀. Pictorially in Figure 3 and quantitatively in Table 2, it emerges that when the mutation determines a gain in the $\Delta G_{\text{binding}}$ there is an increase in the surface complementarity (compare Figure 3b and Figure 3a) and in the ΔSASA value, otherwise when the mutation determines a loss in the $\Delta G_{\text{binding}}$ there is a decrease in the surface complementarity (compare Figure 3c and Figure 3a) and in the ΔSASA value.

In N103W and wt-lysozyme, the position of C₆₀ is the same. In the N46W, the mutation triggers a variation of the fullerene location in the lysozyme binding pocket, which is ultimately responsible for the decrease of the binding energy.

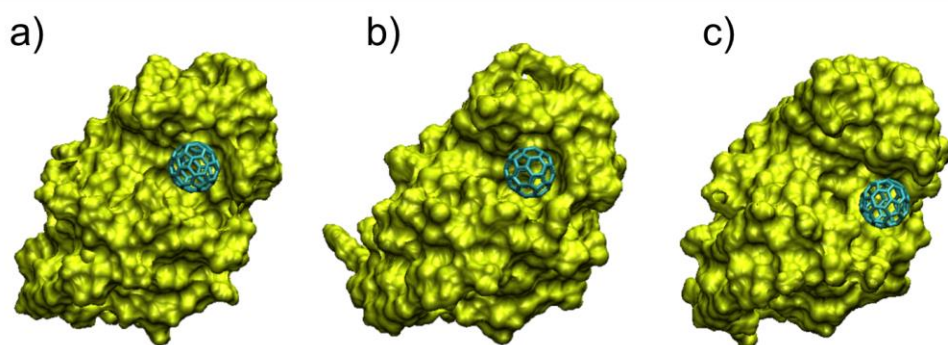


Figure 3. Surface complementarity between the C₆₀ cage and the surface (in yellow) of a) wild-type lysozyme, b) N103W mutant, c) N46W mutant.

Table 2. Estimate of ΔSASA for the wt-lysozyme and mutants upon C₆₀ binding.

Protein	ΔSASA (\AA^2)	$\Delta \text{\AA}^2$ vs wt-lysozyme (\AA^2)
WT	302	–
N103W	315	+13
N46W	282	-20

Optimization of the protein- C_{60} interaction: the case of the N103W mutant

In the case of N103W, $\Delta G_{\text{binding}}$ between C_{60} and N103W is $-22.9 \text{ kcal mol}^{-1}$, which corresponds to an increase of $4.4 \text{ kcal mol}^{-1}$ with respect to wild-type lysozyme.

Analysis of the binding components of the energy (Figure 4a) shows that van der Waals interactions are the driving force of the binding ($-48.4 \text{ kcal mol}^{-1}$).

Hydrophobic interactions, i.e., nonpolar solvation, assist the binding, even if the corresponding value ($-4.5 \text{ kcal mol}^{-1}$) is far smaller than that of van der Waals interactions. Polar solvation is detrimental to the binding and the contribution is positive ($+12.0 \text{ kcal mol}^{-1}$). C_{60} occupies part of the active site of the lysozyme that is made up by many hydrophilic residues: upon formation of the complex with C_{60} , they are forcedly desolvated, destabilizing the system.

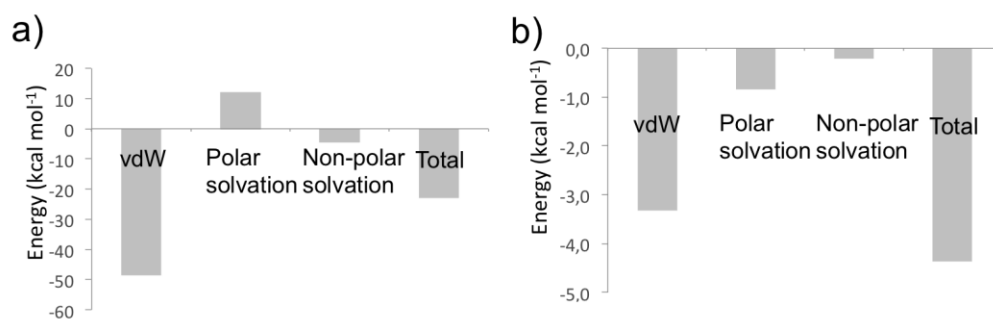


Figure 4. Energy components of $\Delta G_{\text{binding}}$ for C_{60} binding with a) N103W, b)

$\Delta\Delta G_{\text{binding}}$ with respect to the complex of wild-type lysozyme. The data are obtained with a simulation of 100 ns.

The trend of the energy components of the $\Delta G_{\text{binding}}$ of C_{60} for N103W is similar to that of the complex of wild-type lysozyme/ C_{60} . Figure 4b shows that there is an energy gain for all three contributions. The increase of van der Waals and non-polar

solvation terms can be explained with an increase of the shape complementarity between the protein and C₆₀. The Trp 103 is closer to the fullerene cage than Arg 103 (the shortest distances are 3.55 Å for the Trp vs 4.04 Å for Arg) and interacts strongly (Figure 5) with *via* additional π - π interactions (sandwich-like as evidenced in Figure 5b).

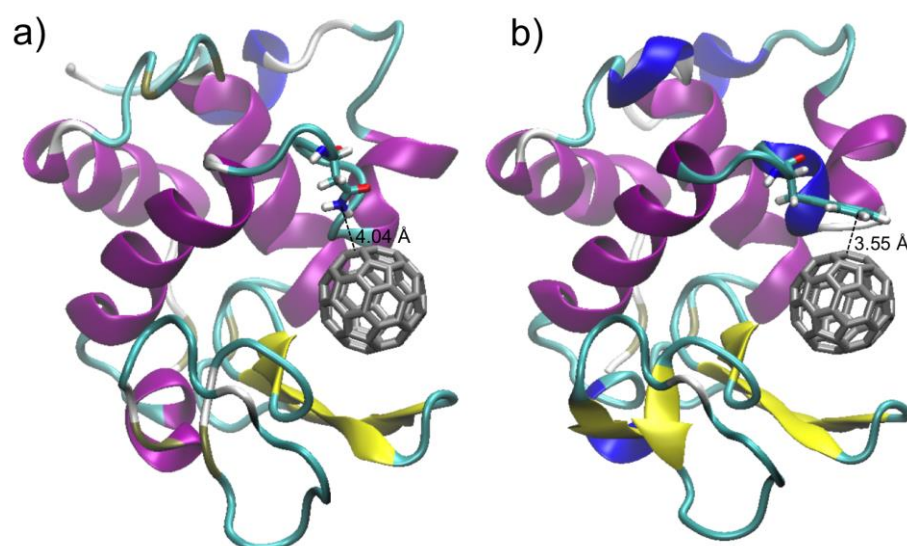


Figure 5. Interaction between Asn103 (a) and Trp103 (b) with C₆₀.

On the other side, the gain in the polar solvation energy is due to the reduction of the polar term, which remains positive. In fact in the wild-type lysozyme during the formation of the complex with C₆₀ the hydrophilic part of asparagine (N103) faces the fullerene cage (see Figure 5a) and is desolvated. This causes a destabilization of the system, because the N103 residue, in the presence of the hydrophobic C₆₀ molecule, is no longer able to interact with water molecules, usually present in the binding pocket, reducing its solvation energy. In the N103W mutant, this energy penalty is reduced, due to the more hydrophobic character of the Trp mutant that faces C₆₀ with its hydrophobic indolic ring, gaining energy and eliminating the desolvation energy penalty due to the C₆₀ binding.

Decrease of the protein- C_{60} interaction: the case of N46W mutant

Figure 3c shows that in N46W the Trp mutation triggers a variation of the fullerene location in the lysozyme binding pocket. The difference is more evident by superimposing the optimized complex of C_{60} with wild type lysozyme and N46W mutant (Figure 6a). In the N46W mutant, the bulkier Trp partly occupies the original fullerene-binding pocket and, as a consequence, C_{60} changes position.

The physiological substrate of lysozyme is a polysaccharide. The recognition pocket consists of six subsites, designated as “A” to “F”, which can accommodate six sugar moieties. In practice, the recognition pocket is a crevice. In wild type lysozyme, C_{60} binds in this crevice.²⁴ Upon the Trp mutation in position 46, the C_{60} molecule slides along the trench. Trp 62 works as a gate and changes its conformation during the sliding of the C_{60} , as evidenced in Figure 6a. In Figure 6b and 6c the two possible sub-pockets that can host the C_{60} molecule and the role of Trp 62 as a gate are highlighted.

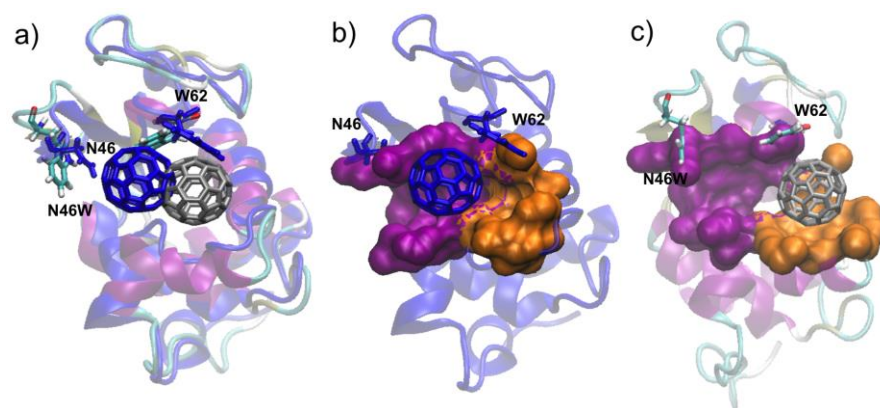


Figure 6. a) Superimposition of the complexes between C_{60} and wild-type lysozyme (in blue) and N46W mutant (in grey). Representation of the two sub-pockets (in purple and orange), able to host C_{60} in b) wild-type lysozyme, c) N46W mutant. The surface of the sub-pockets are calculated using DoGSiteScorer,⁴⁶ a tool for automated pocket detection and analysis.

The analysis of the root-mean square displacement of the center of mass of the C₆₀ molecule (Figure 7) during the MD trajectories, allows quantification of the mobility of the C₆₀ in complex with N46W, especially if compared with wild type lysozyme and N103W.

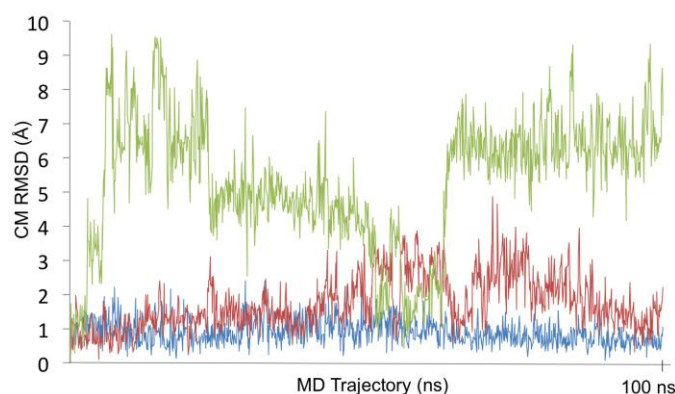


Figure 7. Root-mean square displacement of the center of mass of the C₆₀ during the MD trajectory of the C₆₀ complex with wild-type lysozyme (blue line), N103W (red line) and N46W (green line).

In the wild type enzyme and in N103W, C₆₀ remains in its binding pocket during the entire trajectory, apart for a small local re-arrangement in the mutant. In the N46W, C₆₀ hops between two sub-pockets.

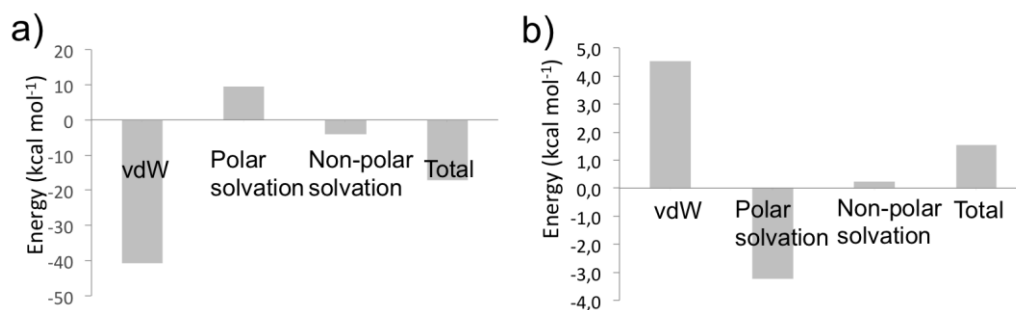


Figure 8. a) Energy components of the $\Delta G_{\text{binding}}$ for C₆₀ binding to N46W, b) $\Delta\Delta G_{\text{binding}}$ with respect to the complex of wild-type lysozyme. The data are obtained with a simulation of 100 ns.

Compared to the shorter simulation of 10 ns, the energy difference/loss upon binding of C₆₀ is smaller since the longer simulation allows the protein to re-organize locally (Figure 8a). This is probably due to the fact that for such a particular mutation, C₆₀ shifts to occupy a different position in the protein binding site. This effect strongly affects the final ΔG value.

With respect to the wild type complex, the energy loss is due to van der Waals and non-polar solvation terms (Figure 8b). It can be explained with a decrease of shape complementarity between the protein and C₆₀, due to the continuous movement of C₆₀. As explained previously in the N46W mutant the bulkier Trp occupies partly the wild type lysozyme fullerene binding pocket, generating a steric clash that decreases the van der Waals interaction energy and the solvent accessible surface area. In a few words the Trp 46 continuously “kicks” the C₆₀ ball to a different sub-pocket. Also the positive effect of the mutation on the polar solvation term is due to the position changing of C₆₀. In fact the wild type lysozyme binding pocket is made up by many hydrophilic residues, when C₆₀ moves from the wild type pocket to the other sub-pocket these residues became, as before the C₆₀ binding, solvent-exposed and increase the solvation term. However, even if important ($-3.2 \text{ kcal mol}^{-1}$), this term energetically do not balance the detrimental variations.

3. Conclusion

In this paper, we have showed that it is possible to use computational protein design to understand and optimize protein-binding pockets that bind to the π -electron rich

surface of fullerenes. In particular, the approach was used to engineer the binding pocket of lysozyme to host a C₆₀ molecule. The presence of amino acids with a strong tendency to bind carbon nanoparticles, such as Trp, does not suffice *per se* to guarantee the improvement of the binding of proteins to fullerene. In fact to increase $\Delta G_{\text{binding}}$ a crucial role is played by the location where Trp residues are positioned since mutation of residues in wild type proteins may trigger small structural variations that lead to destabilization of the complex between C₆₀ and the protein.

4. Computational Details

In silico generation of the mutants. Experimental data from NMR²⁴ and a docking protocol^{6,8,14,16,24,47} recently validated for the study of interaction between proteins and nanoobjects were used to generate the initial coordinates of the adduct between protein and C₆₀ as previously described.^{6,8,14,16,24,47} The lateral chain of the residue to be mutated is deleted in the pdb file and the Trp residue is added using the *tLeap* module in antechamber.⁴⁹ Only to remove severe sterical clashes, the position of the added Trp residues in all the mutants are optimized with SANDER, with the C₆₀ and all the protein atoms (except the mutated Trp) frozen.

Setting the Simulation. Chloride counterions were included to exactly neutralize the positively charged lysozyme mutants. All simulations were performed with explicit solvent by using the TIP3P water model (7605 water molecules).⁴⁸ The same water box was used for all the simulation. The ff10 force field was used to model lysozyme mutants.⁴⁹ The C₆₀ atoms were modeled as uncharged Lennard–Jones particles by using sp² carbon parameters from the ff10 force field.⁴⁹

Minimization and Equilibration. About 10,000 steps of steepest descent minimization were performed for the whole system with PMEMD.⁴⁹ The minimized

structure was considered for a 3 step equilibration protocol. Particle Mesh Ewald summation⁴⁹ was used throughout (cut off radius of 10 Å for the direct space sum). H atoms were considered by the SHAKE algorithm⁴⁹ and a time step of 2 fs was applied in all MD runs. Individual equilibration steps included (i) 50 ps of heating to 298 K within an NVT ensemble and temperature coupling according to Berendsen. (ii) 50 ps of equilibration MD at 298 K to switch from NVT to NPT and adjust the simulation box. Isotropic position scaling was used at default conditions. (iii) 900 ps of continued equilibration MD at 298 K for an NPT ensemble switching to temperature coupling according to Andersen.

Production MD. MD simulation was carried out for the equilibrated system using PMEMD.⁴⁹ Simulation conditions were identical to the final equilibration step (iii). Overall sampling time was 10 ns for all the mutants. Two longer trajectory of 100 ns were carried out for the N46W and N103W mutants.

Post Processing of Trajectories, MM-PBSA Molecular Mechanics/ Generalized Born Surface Area. MM-GBSA^{50,51} analysis was carried out to estimate the binding free energy of the C₆₀ when complexed to lysozyme mutants. MM/GBSA analysis is a postprocessing method in which representative snapshots from an ensemble of conformations are used to calculate the free energy change between two states (typically a bound and free state of a receptor and a ligand).⁵⁰ Free energy differences are calculated by combining the gas phase energy contributions that are independent of the solvent model as well as solvation free energy components (both polar and nonpolar) calculated from an implicit solvent model for each species.⁵¹ The molecular mechanics energies are determined with the SANDER program from Amber⁴⁹ and represent the internal energy (bond, angle and dihedral), and van der Waals and electrostatic interactions. An infinite cutoff for all interactions is used. The

electrostatic contribution to the solvation free energy is calculated by generalized Born (GB) methods implemented in SANDER. The nonpolar contribution to the solvation free energy has been determined with solvent-accessible surface-area dependent terms. Individual snapshot structures of all trajectories were analyzed with the program PTRAJ.⁴⁹

Acknowledgements

This study was supported by the Italian Ministry of Education, University and Research MIUR - SIR Programme no. RBSI149ZN9-BIOTAXI funded to MC.

References

- [1] a) A. E. Nel, L. Mädler, D. Velegol, T. Xia, E. M. V. Hoek, P. Somasundaran, F. Klaessig, V. Castranova, M. Thompson, *Nat. Mater.* **2009**, 8, 543-557; b) S. Rana, Y.-C. Yeh, V. M. Rotello, *Curr. Opin. Chem. Biol.* **2010**, 14, 828-834; c) J. E. Gagner, S. Shrivastava, X. Qian, J. S. Dordick, R. W. Siegel *J. Phys. Chem. Lett.* **2012**, 3, 3149-3158
- [2] M. Calvaresi, F. Zerbetto, *Acc. Chem. Res.* **2013**, 46, 2454-2463.
- [3] a) L. L. Looger, M. A. Dwyer, J. J. Smith, H. W. Hellinga, *Nature* **2003**, 423, 185-190; b) S. M. Lippow, B. Tidor, *Curr. Opin. Biotechnol.* **2007**, 18, 1-7; c) C. Malisi, M. Schumann, N. C. Toussaint, J. Kageyama, O. Kohlbacher, B. Hocker, *Plos One* **2012**, 7, e52505, d) C. E. Tinberg, S. D. Khare, J. Dou, L. Doyle, J. W. Nelson, A. Schena, W. Jankowski, C. G. Kalodimos, K. Johnsson, B. L. Stoddard, D. Baker, *Nature* **2013**, 501, 212-216; e) M. M. Pakulska, S. Miersch, M. S. Shoichet, *Science* **2016**, 351, aac4750.

- [4] S. H. Friedman, D. L. DeCamp, R. P. Sijbesma, G. Srdanov, F. Wudl, G. L. Kenyon, *J. Am. Chem. Soc.* **1993**, *115*, 6506-6509.
- [5] M. Junaid, E. A. Almuqri, J. Liu, H. Zhang, *Plos One* **2016**, *11*, e0147761.
- [6] M. Calvaresi, A. Bottoni, F. Zerbetto, *J. Phys. Chem. C* **2015**, *119*, 28077-28082.
- [7] G. Leonis, A. Avramopoulos, K. D. Papavasileiou, H. Reis, T. Steinbrecher, M. G. Papadopoulos, *J. Phys. Chem. B* **2015**, *119*, 14971-14985.
- [8] M. Calvaresi, S. Furini, C. Domene, A. Bottoni, F. Zerbetto, *ACS Nano* **2015**, *9*, 4827-4834.
- [9] M. Turabekova, B. Rasulev, M. Theodore, J. Jackman, D. Leszczynski, J. Leszczynski, *Nanoscale* **2014**, *6*, 3488-3495.
- [10] S. Radic, P. Nedumpully-Govindan, R. Chen, E. Salonen, J. M. Brown, P. C. Ke, F. Ding, *Nanoscale* **2014**, *6*, 8340–8349.
- [11] P. N. Govindan, L. Monticelli, E. Salonen, *J. Phys. Chem. B* **2012**, *116*, 10676-10683.
- [12] L. Monticelli, J. Barnoud, A. Orlowski, I. Vattulainen, *Phys. Chem. Chem. Phys.* **2012**, *14*, 12526-12533.
- [13] S. G. Kang, T. Huynh, R. H. Zhou, *Sci. Rep.* **2012**, *2*, 957.
- [14] M. Calvaresi, F. Zerbetto, *Nanoscale* **2011**, *3*, 2873-2881.
- [15] G. Zuo, X. Zhou, Q. Huang, H. Fang, R. Zhou, *J. Phys. Chem. C* **2011**, *115*, 23323-23328.
- [16] M. Calvaresi, F. Zerbetto, *ACS Nano* **2010**, *4*, 2283-2299.
- [17] S. Kraszewski, M. Tarek, W. Treptow, C. Ramseyer, *ACS Nano* **2010**, *4*, 4158-4164.
- [18] X. Wu, S.-T. Yang, H. Wang, L. Wang, W. Hu, A. Cao, Y. Liu, *J. Nanosci. Nanotechnol.* **2010**, *10*, 6298-6304.

- [19] H. Benyamini, A. Shulman-Peleg, H. J. Wolfson, B. Belgorodsky, L. Fadeev, M. Gozin, *Bioconjugate Chem.* **2006**, *17*, 378-386.
- [20] S. J. Vance, V. Desai, B. O. Smith, M. W. Kennedy, A. Cooper, *Biophys. Chem.* **2016**, *214-215*, 27-32.
- [21] K.-H. Kim, D.-K. Ko, Y.-T. Kim, N. H. Kim, J. Paul, S.-Q. Zhang, C. B. Murray, R. Acharya, W. F. DeGrado, Y. H. Kim, G. Grigoryan, *Nat. Commun.* **2016**, *7*, 11429.
- [22] Y. Pan, L. Wang, S. Kang, Y. Lu, Z. Yang, T. Huynh, C. Chen, R. Zhou, M. Guo, Y. Zhao, *ACS Nano* **2015**, *9*, 6826-6836.
- [23] S. Zanzoni, A. Ceccon, M. Assfalg, R. K. Singh, D. Fushman, M. D'Onofrio, *Nanoscale* **2015**, *7*, 7197-7205.
- [24] M. Calvaresi, F. Arnesano, S. Bonacchi, A. Bottoni, V. Calò, S. Conte, G. Falini, S. Fermani, M. Losacco, M. Montalti, G. Natile, L. Prodi, F. Sparla, F. Zerbetto, *ACS Nano*, **2014**, *8*, 1871-1877.
- [25] Y. Miao, J. Xu, Y. Shen, L. Chen, Y. Bian, Y. Hu, W. Zhou, F. Zheng, N. Man, Y. Shen et al. *ACS Nano* **2014**, *8*, 6131-6144.
- [26] P. Chen, S. A. Seabrook, V. C. Epa, K. Kurabayashi, A. S. Barnard, D. A. Winkler, J. K. Kirby, P. C. Ke, *J. Phys. Chem. C* **2014**, *118*, 22069-22078.
- [27] E. Mentovich, B. Belgorodsky, M. Gozin, S. Richter, H. Cohen, *J. Am. Chem. Soc.* **2012**, *134*, 8468-8473.
- [28] S. G. Kang, G. Zhou, P. Yang, Y. Liu, B. Sun, T. Huynh, H. Meng, L. Zhao, G. Xing, C. Chen, et al. *Proc. Natl. Acad. Sci. U. S. A.* **2012**, *109*, 15431-15436.
- [29] M. Zhen, J. Zheng, L. Ye, S. Li, C. Jin, K. Li, D. Qiu, H. Han, C. Shu, Y. Yang, et al. *ACS Appl. Mater. Interfaces* **2012**, *4*, 3724-3729.
- [30] H. Wu, L. Lin, P. Wang, S. Jiang, Z. Dai, X. Zou, *Chem. Commun.* **2011**, *47*, 10659-10661.

- [31] T. A. Ratnikova, P. N. Govindan, E. Salonen, P. C. Ke, *ACS Nano* **2011**, *5*, 6306-6314.
- [32] S. Maoyong, J. Guibin, Y. Junfa, W. Hailin, *Chem. Commun.* **2010**, *46*, 1404-1406.
- [33] A. Innocenti, S. Durdagi, N. Doostdar, A. T. Strom, A. R. Barron, C. T. Supuran, *Bioorg. Med. Chem.* **2010**, *18*, 2822-2828.
- [34] S. Durdagi, C. T. Supuran, T. A. Strom, N. Doostdar, M. K. Kumar, A. R. Barron, T. Mavromoustakos, M. G. Papadopoulos, *J. Chem. Inf. Model.* **2009**, *49*, 1139-1143.
- [35] S.-T. Yang, H. Wang, L. Guo, Y. Gao, Y. Liu, A. Cao, *Nanotechnology* **2008**, *19*, 395101.
- [36] X. Zhang, C. Shu, L. Xie, C. Wang, Y. Zhang, J. Xiang, L. Li, Y. Tang, *J. Phys. Chem. C* **2007**, *111*, 14327-14333.
- [37] G. Pastorin, S. Marchesan, J. Hoebeke, T. Da Ros, L. Ehret-Sabatier, J.-P. Briand, M. Prato, A. Bianco, *A. Org. Biomol. Chem.* **2006**, *4*, 2556-2562.
- [38] B. Belgorodsky, L. Fadeev, J. Kolsenik, M. Gozin, *ChemBioChem* **2006**, *7*, 1783-1789.
- [39] B. Belgorodsky, L. Fadeev, V. Ittah, H. Benyamini, S. Zelner, D. Huppert, A. B. Kotlyar, M. Gozin, *Bioconjugate Chem.* **2005**, *16*, 1058-1062.
- [40] T. Mashino, K. Shimotohno, N. Ikegami, D. Nishikawa, K. Okuda, K. Takahashi, S. Nakamura, M. Mochizuki, *Bioorg. Med. Chem. Lett.* **2005**, *15*, 1107-1109.
- [41] K. H. Park, M. Chhowalla, Z. Iqbal, F. Sesti, *J. Biol. Chem.* **2003**, *278*, 50212-50216.
- [42] M. Calvaresi, F. Zerbetto, *J. Mater. Chem. A* **2014**, *2*, 12123-21135.

- [43] M. Calvaresi, F. Zerbetto, *Chem.-Eur. J.* **2012**, *18*, 4308-4313.
- [44] a) V. Zorbas, A. L. Smith, H. Xie, A. Ortiz-Acevedo, A. Dalton, G. R. Dieckmann, R. K. Draper, R. H. Baughman, I. Musselman, *J. Am. Chem. Soc.* **2005**, *127*, 12323-12328; b) H. Xie, E. J. Becraft, R. H. Baughman, A. B. Dalton, G. R. Dieckmann, *J. Pept. Sci.* **2008**, *14*, 139-151; c) S. M. Tomasio, T. R. Walsh, *J. Phys. Chem. C* **2009**, *113*, 8778-8785; d) L. Zheng, D. Jain, P. Burke, *J. Phys. Chem. C* **2009**, *113*, 3978-3985.
- [45] a) D. Canevet, E. M. Perez, N. Martin, *Angew. Chem., Int. Ed.* **2011**, *50*, 9248-9259; b) E. M. Perez, N. Martin, *Chem. Soc. Rev.* **2008**, *37*, 1512-1519.
- [46] A. Volkamer, A. Griewel, T. Grombacher, M. Rarey, *J. Chem. Inf. Model.* **2010**, *50*, 2041-2052
- [47] M. Calvaresi, F. Zerbetto, *J. Chem. Inf. Model.* **2011**, *51*, 1882-1896.
- [48] W. L. Jorgensen, J. Chandrasekhar, J. D. Madura, R. W. Impey, M. L. Klein, *J. Chem. Phys.* **1983**, *79*, 926-935.
- [49] D. A. Case, T. E. Cheatham, III; T. Darden, H. Gohlke, R. Luo, K. M. Merz, Jr. A. Onufriev, C. Simmerling, B. Wang, R. Woods, *J. Comput. Chem.* **2005**, *26*, 1668-1688.
- [50] P. A. Kollman, I. Massova, C. Reyes, B. Kuhn, S. Huo, L. Chong, M. Lee, T. Lee, Y. Duan, W. Wang, et al. *Acc. Chem. Res.* **2000**, *33*, 889-897.
- [51] B. R. Miller, III; T. D. McGee, Jr.; J. M. Swails, N. Homeyer, H. Gohlke, A. E. Roitberg, *J. Chem. Theory Comput.* **2012**, *8*, 3314-3321.